

Title	Direct oxidation of ammonia borane as an alternative fuel at nanoporous Au
Authors	Nagle, Lorraine C.;Rohan, James F.
Publication date	2010-01
Original Citation	Nagle, L. C. and Rohan, J. F. (2010) 'Direct Oxidation of Ammonia Borane as an Alternative Fuel at Nanoporous Au', ECS Transactions, 25 (41), pp. 13-25. doi: 10.1149/1.3422496
Type of publication	Article (peer-reviewed)
Link to publisher's version	http://ecst.ecsdl.org/content/25/41/13 - 10.1149/1.3422496
Rights	© 2010 ECS - The Electrochemical Society
Download date	2025-05-12 22:39:20
Item downloaded from	https://hdl.handle.net/10468/7603



UCC

University College Cork, Ireland
Coláiste na hOllscoile Corcaigh

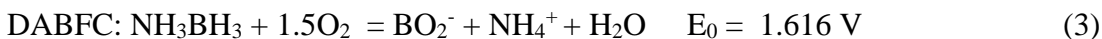
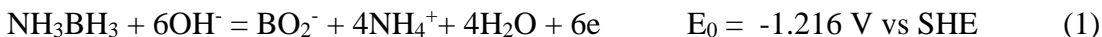
Direct Oxidation of Ammonia Borane as an Alternative Fuel at Nanoporous Au

L. C. Nagle and J. F. Rohan.

Tyndall National Institute, University College Cork, Lee Maltings,
Prospect Row, Cork, Ireland

Introduction

Ammonia borane (AB) is a chemically stable, non-toxic solid with a high hydrogen content (19.5 wt. %) which is easily transported and is highly soluble in water. It has been shown that hydrogen can be released from AB via catalytic hydrolysis (1-6) or thermal decomposition (7-10). It can thermally decompose in the temperature range 340-410 K to liberate 2.2 mol H₂ per mol of AB which is equivalent to a hydrogen storage density of 14.3 wt. %. The high energy density coupled with the moderate decomposition temperature make AB an attractive hydrogen source for fuel cells. However, if the *direct* electrochemical oxidation of AB occurs in a fuel cell a more negative potential and greater power can be obtained than indirectly using hydrogen as the fuel (11, 12). A novel direct AB fuel cell (DABFC) can be proposed by combining the anodic oxidation of AB given by Eqn. 1 and cathodic reduction of oxygen (Eqn. 2).



The direct electro-oxidation of AB (Eqn. 1) has been investigated at a Au microdisc (13) and Au disc electrodes in alkaline media (5). Establishing a technology for a DABFC hinges on understanding the mechanism and kinetics of this reaction and the associated catalytic species at the anode. Careful selection of the anode catalyst is crucial in minimising competing hydrolysis given by Eqn. 4 resulting in heterogeneous, non-faradaic hydrogen evolution which decreases fuel utilisation and lowers cell performance.



Au is an effective catalyst for AB oxidation and is non-catalytic with respect to its hydrolysis. In this paper we report on the exploitation of nanoporous Au with high specific surface area and electrocatalytic activity to develop an anode catalyst with high catalytic activity for oxidation of ammonia borane and low activity for its hydrolysis.

Nanoporous Au (NPG) can be formed by a chemical etching process called dealloying which involves selective metal dissolution. This has an ancient history. Incan civilisation dealloyed Cu from surface of Cu-Au alloys to create an illusion of a pure Au artefact known as depletion gilding. In the 1970s Forty (14) showed that depletion gilding of a less-noble metal from Au alloys results in an open, continuous nanoporous structure composed of Au. As the Ag atoms in an Ag_xAu_y alloy are dissolved in acid, remaining Au atoms gather

together in clusters that create a rough surface causing Au to evolve into a porous material. Dealloyed Au atoms act like water droplets condensed on a pane of glass – the Au atoms condense into little clumps that grow into the backbone of a porous structure. The sponge-like 3D structure is a system of interconnecting pores/tunnels in a skeleton of filaments of the metal. The filament size can range from 5-50 nm and surface areas as high as $20 \text{ m}^2 \text{ g}^{-1}$ with a porosity of 70 % or higher are possible. NPG is mechanically far stronger than is supposed on the basis of a scaling law, presumably because the ligament size in the nm range causes dislocation starvation. Structurally it bears a resemblance to naturally occurring zeolites (filament size 1-2 nm and surface areas $100 \text{ m}^2 \text{ g}^{-1}$ (15). This is a useful but relatively unstudied form of Au that likely contains an intrinsically high step density. Given that NPG has an interconnected, bicontinuous ligament network containing regions of both negative and positive curvature, a high step density is topologically required. This characteristic makes NPG attractive for catalysis studies; it is made even more attractive because it can be easily formed into thin, high-conductivity foils that are easily adapted to electrocatalytic measurements. In terms of catalytic applications, NPG has at least two advantages over other catalysts or Au nanoparticles. Firstly, unlike Pt or Pd catalysts, NPG remains active at low temperature (room temperature or even lower), which is desirable for many practical applications. Secondly, NPG has a good thermal stability and is resistant to oxidation and thus can overcome the aggregation or sintering limitations from which Au nanoparticles often suffer upon the elevation of temperature or in an oxidative environment. Low Temperature CO Oxidation over unsupported NPG was shown by Xu et al. (16). NPG in a foam type structure has been shown to exhibit high CO oxidation activity, however the catalytic reactions only occur at the surfaces of NPG foams (17). Zeis et al. (18) demonstrated that NPG is an effective catalyst for the reduction of hydrogen peroxide to water. The reaction efficiency is sufficiently high to allow use of the material as a cathode for oxygen reduction in hydrogen PEM fuel cells, although the overall efficiency in this context is still far less efficient than that of Pt. Their results are consistent with their overall hypothesis that the central difference between NPG and bulk Au is due to the increased density of step edges in NPG overall bulk Au. Generally, however, it is important to note how that the pace of discovery of the number of reactions for which NPG by itself is a good catalyst is rapidly increasing, and many different systems in which NPG may be the superior catalyst remains to be examined.

Experimental

The borane complex utilized in this work, AB (minimum purity 97%) and sodium hydroxide, NaOH (minimum purity 99%) were purchased from Sigma Aldrich and used as received. Deionized water of resistivity $18 \text{ M}\Omega \text{ cm}$ was used to prepare all solutions. The working electrodes were a $10 \text{ }\mu\text{m}$ diameter Au microdisk (Princeton Applied Research) and a 5 mm Au disc (Princeton Applied Research) supplied by Advanced Measurement Technology, U.K. These were polished with $0.5 \mu\text{m}$ alumina powder obtained from Struers on a Buehler polishing cloth for 1–2 min and rinsed in deionized water. A 1 mm diameter Au counter electrode of 50 mm length was used, Cyclic voltammograms (CV) were recorded with respect to a standard calomel electrode. The potential of the working electrode was controlled using a CH Instruments potentiostat model 660B with picoamp booster. All solutions were purged with nitrogen for 20 min prior to experiments in order to remove oxygen, and the experiments were performed at $20 \text{ }^\circ\text{C}$. TEM images were recorded using JEOL 2000FX at an accelerating voltage of 200 kV. SEM images were recorded using Nova Nanosem 630 at an accelerating voltage of 15 kV.

Results and Discussion

The electrochemistry of AB at planar Au

Typical behaviour for Au in 1 M NaOH is seen in the CV recorded for a microdisc electrode shown in Fig 1. This voltammogram shows that negligible current flows in the absence of AB over the potential range -1.0 to $+0.05$ V. The onset of monolayer oxide formation is shown to occur above $+0.05$ V with the corresponding oxide reduction peak on the reverse sweep.

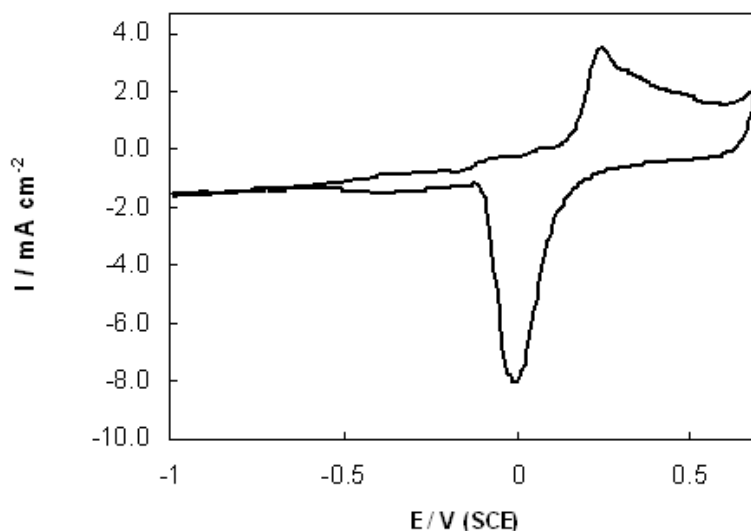


Figure 1. Cyclic voltammogram for a Au microdisc ($r = 5 \mu\text{m}$) in 1.0 mol dm^{-3} NaOH at 10 mV s^{-1} .

When 20 mM AB is added to the 1 M NaOH solution, a well-defined CV shown in Fig. 2 is achieved consisting of two irreversible anodic waves. Mass transport controlled steady-state currents were recorded for the first and second waves at -0.95 and -0.12 V, respectively. The voltammograms exhibit a pronounced plateau region upon sweeping the potentials to more positive values. The current then decreases as the potential is swept into the Au monolayer oxide region.

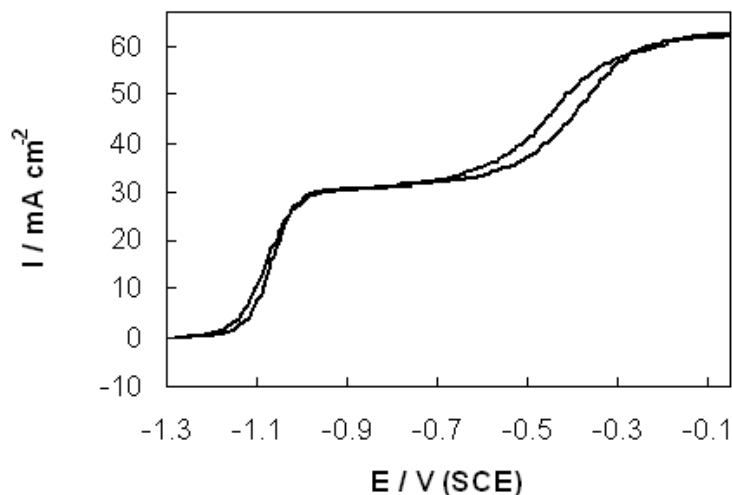


Figure 2. Cyclic voltammogram for a Au microdisc in 1.0 mol dm⁻³ NaOH containing 0.02 mol dm⁻³ AB at 10 mV s⁻¹.

Typical behaviour for Au in 1 M NaOH is seen in the CV recorded for a Au disc electrode shown in Fig. 3. This voltammogram shows that negligible current flows in the absence of AB over the potential range -0.9 to +0.05 V. When 20 mM AB is added to the 1 M NaOH solution, the CV shown in Fig. 4 is achieved. The voltammograms exhibit a pronounced plateau region upon sweeping the potentials to more positive values, the current then decreases as the potential is swept into the Au monolayer oxide region. A single irreversible anodic wave was observed, it was not possible to resolve this into the two irreversible anodic waves that were recorded at the Au microdisc (see Fig.2).

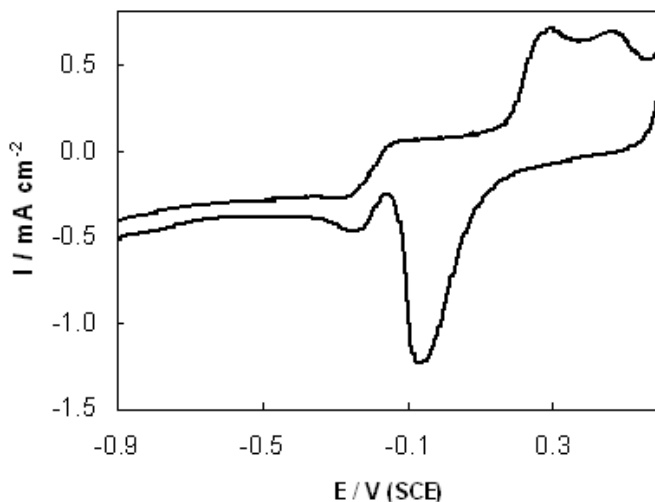


Figure 3. Cyclic voltammogram for a Au disc electrode in 1.0 mol dm⁻³ NaOH at 10 mV s⁻¹.

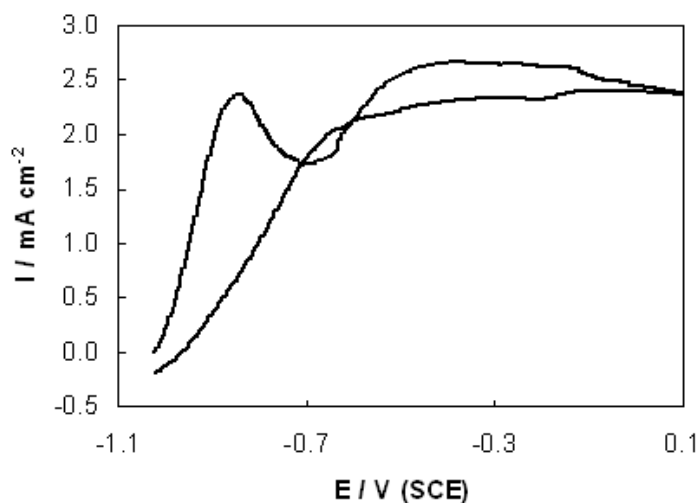


Figure 4. Cyclic voltammogram for a Au RDE in 1.0 mol dm⁻³ NaOH containing 0.02 mol dm⁻³ AB at 10 mV s⁻¹.

Fabrication of NPG on a planar Au film

Ag_xAu_y films were deposited on a 200 nm Au film on pyrex at constant potential of -1.2 V from a solution of 100 mM $\text{KAg}(\text{CN})_2$ and 20 mM $\text{KAu}(\text{CN})_2$ in 250 mM Na_2CO_3 , pH 13 for 20 mins. EDX confirmed that an alloy composition of $\text{Au}_{0.28}\text{Ag}_{0.82}$ was formed. The CV response recorded for the alloy in 2 M NaOH from -0.9 to 0.6 V vs SCE at 10 mV s^{-1} (not shown here) indicated the presence of Au and Ag from the metal oxide reduction peaks seen at -0.1 V and 0.4 V, respectively. Upon immersing the $\text{Au}_{0.28}\text{Ag}_{0.82}$ in 30 % nitric acid for 15 min a high surface area form of Au referred to as NPG is obtained. The NPG film was delaminated from the underlying Au film and sandwiched in a holey Cu folding TEM grid in order to obtain the TEM image shown in Fig. 5. The pore and ligament size are 20 nm and 30 nm, respectively.

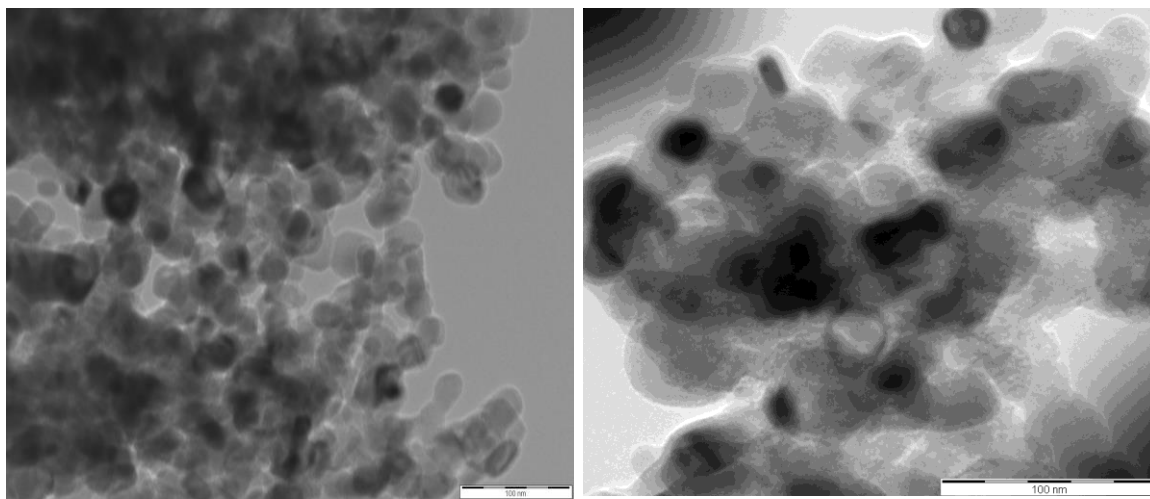


Figure 5. TEM image of NPG.

Fabrication of NPG in 3D wire array

The fabrication of a NPG in a 3D wire array format was achieved by dealloying Ag_xAu_y nanowires that were deposited in Anodisc alumina membranes with 200 nm pore size using the conditions given above for the fabrication of NPG on a planar Au film. The alumina membrane had a conducting backing layer of 350 nm Au which was sputter deposited. The alumina was dissolved by soaking it in 0.5 M NaOH for 2 hours to release the NPG wires. The SEM image shown in Fig.6 was recorded for the resulting NPG wires.

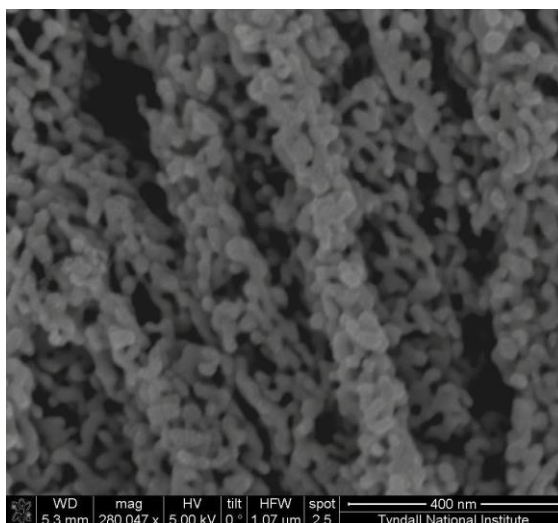


Figure 6. SEM image of NPG wire array on Au

It was attempted to add structural rigidity to the NPG wires by depositing (i) a NPG coating on a Au wire array and (ii) NPG wires onto the ends of a Au wire array, as outlined below. This invariably leads to an increase in the amount of Au used in the electrode fabrication, however.

Fabrication of NPG-coated 3D Au wire array

A 3D Au wire array was deposited in Anodisc alumina membranes with a 350 nm Au conducting backing layer from a commercial Puramet bath. The Au wires were deposited to a length of 1 micron and 200 nm in diameter. The alumina was dissolved by soaking it in 0.5 M NaOH for 2 hours to release the Au wires. The Au wire array was then coated with NPG to a thickness of 20 nm. This was achieved by dealloying Ag_xAu_y nanowires that were deposited on the Au wires using the conditions given above for the fabrication of NPG on a planar Au film. The SEM image shown in Fig. 7 was recorded for the resulting NPG-coated Au wires.

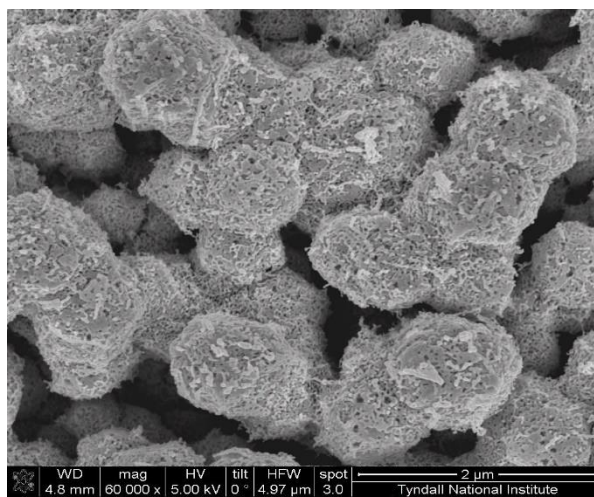


Figure 7. SEM image of NPG-coated Au wire array on Au.

Fabrication of segmented NPG-Au 3D wire array

A 3D Au wire array was deposited in Anodisc alumina membranes with a 350 nm Au conducting backing layer from a commercial Puramet bath. The Au wires were deposited to a length of 3 micron and 200 nm in diameter. The fabrication of NPG onto the Au wires was achieved by dealloying Ag_xAu_y wires that were then deposited on the Au wires in the Anodisc alumina membranes using the conditions given above for the fabrication of NPG on a planar Au film. The alumina was dissolved by soaking it in 0.5 M NaOH for 2 hours to release the segmented Au-NPG wires. The SEM image shown in Fig. 8 was recorded for the resulting segmented NPG-Au 3D wire array.

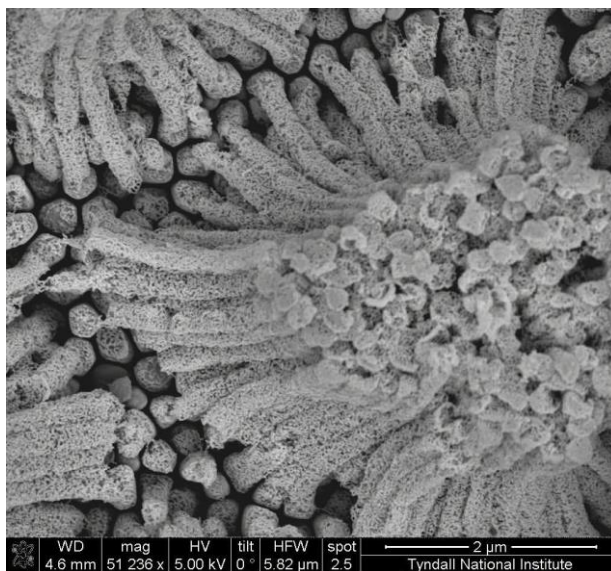


Figure 8. SEM image of segmented NPG-Au nanowire array on Au

The electrochemistry of AB at NPG

The CV response for NPG in 1 M NaOH is shown in Fig. 9. It is estimated from the increase in monolayer oxide reduction current over that at the clean Au disc electrode that the surface area has increased by a factor of 5. When 20 mM AB is added to the 1 M NaOH solution, the CV shown in Fig. 10 is achieved. The onset potential for the oxidation of AB has shifted to a more negative potential of -1.20 V and the oxidation current of 3.1 mA cm^{-2} represents a 24 % increase over that seen at a Au disc electrode.

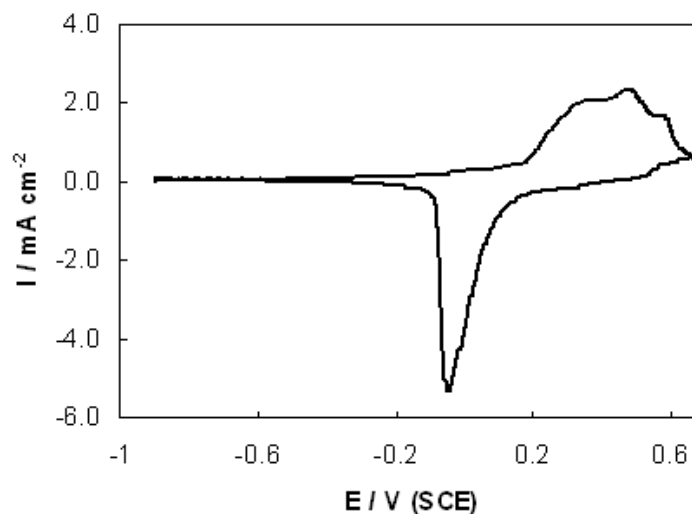


Figure 9. Cyclic voltammogram for NPG on a Au disc electrode in $1.0 \text{ mol dm}^{-3} \text{ NaOH}$ at 10 mV s^{-1}

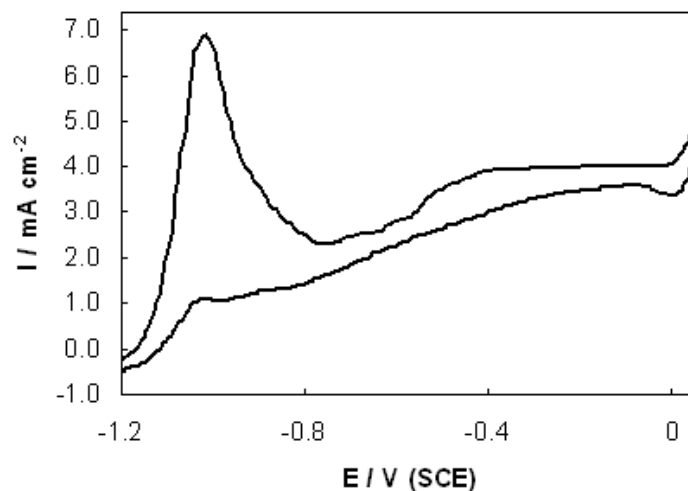


Figure 10. Cyclic voltammogram for NPG on a Au disc electrode in $1.0 \text{ mol dm}^{-3} \text{ NaOH}$ containing $0.02 \text{ mol dm}^{-3} \text{ AB}$ at 10 mV s^{-1}

The CV response for NPG wire array in 1 M NaOH is shown in Fig. 11. It is estimated from the increase in monolayer oxide reduction current over that at a planar Au disc electrode that the surface area increased by a factor of 19. When 20 mM AB is added to the 1 M NaOH solution, the CV shown in Fig. 12 is achieved. The onset potential for the oxidation of AB has shifted to a more negative potential of -1.30 V and the oxidation current of 13.1 mA cm^{-2} represents more than a fivefold increase over that seen at a Au disc electrode.

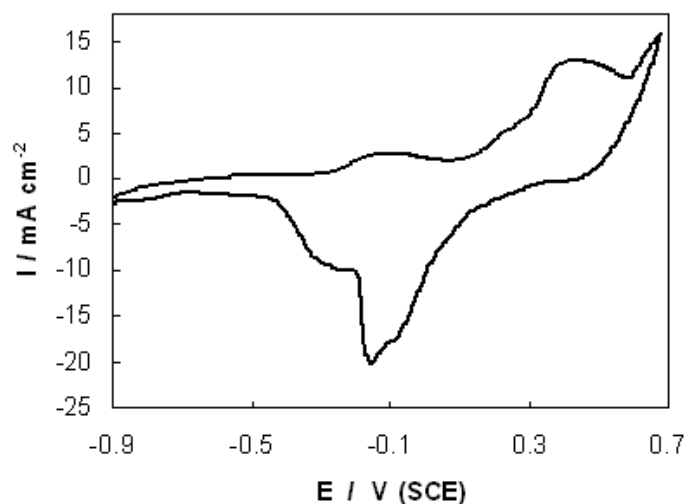


Figure 11. Cyclic voltammogram for NPG wire array on a planar Au film in 1.0 mol dm^{-3} NaOH at 10 mV s^{-1} .

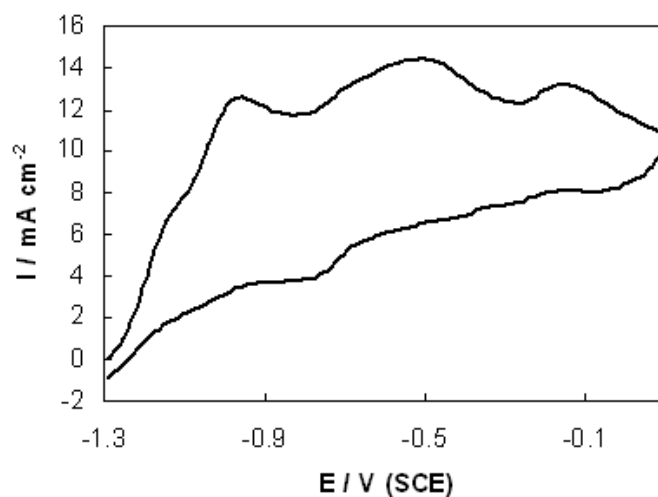


Figure 12. Cyclic voltammogram for NPG wire array on a planar Au film in 1.0 mol dm^{-3} NaOH containing 0.02 mol dm^{-3} AB at 10 mV s^{-1} .

The CV response for a segmented NPG-Au wire array (as indicated in Fig. 8) in 1 M NaOH is shown in Fig. 13. It is estimated from the increase in monolayer oxide reduction current over that at a planar Au disc electrode that the surface area increased by a factor of 40. When 20 mM AB is added to the 1 M NaOH solution, the CV shown in Fig. 14 is achieved. The onset potential for the oxidation of AB is -1.27 V and the oxidation current of 12.8 mA cm^{-2} represents a fivefold increase over that seen at a Au disc electrode.

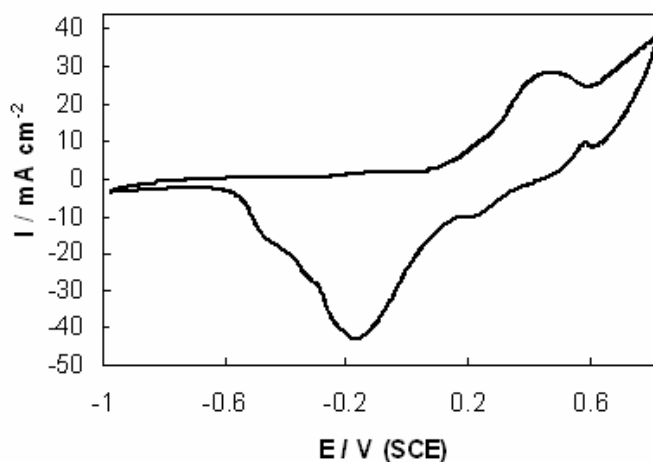


Figure 13. Cyclic voltammogram for segmented NPG-Au wire array on a planar Au film in 1.0 mol dm^{-3} NaOH at 10 mV s^{-1} .



Figure 14. Cyclic voltammogram for segmented NPG-Au wire array on a planar Au film in 1.0 mol dm^{-3} NaOH containing 0.02 mol dm^{-3} AB at 10 mV s^{-1} .

The CV response for NPG-coated Au wire array in 1 M NaOH is shown in Fig. 15. It is estimated from the increase in monolayer oxide reduction current over that at the clean Au disc electrode that the surface area has increased by a factor of 17. When 20 mM AB is added to the 1 M NaOH solution, the CV shown in Fig. 16 is achieved. The onset potential for the oxidation of AB has shifted to a more negative potential of -1.20 V and the oxidation current of 10.5 mA cm^{-2} represents more than a fourfold increase over that seen at a Au disc electrode.

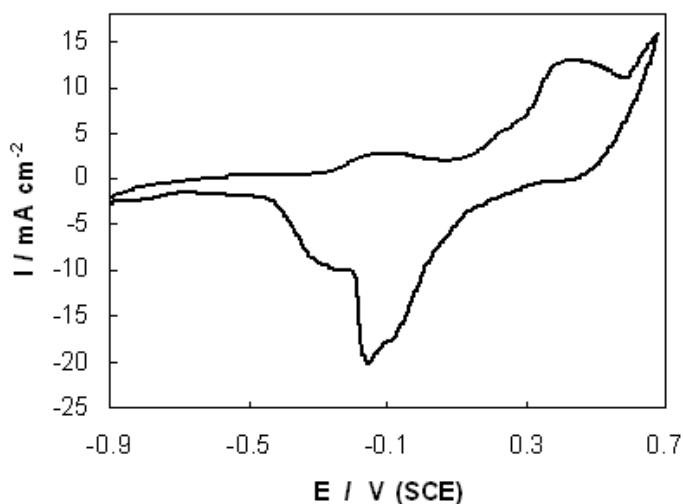


Figure 15. Cyclic voltammogram for NPG-coated Au wire array on a planar Au film in 1.0 mol dm⁻³ NaOH at 10 mV s⁻¹.

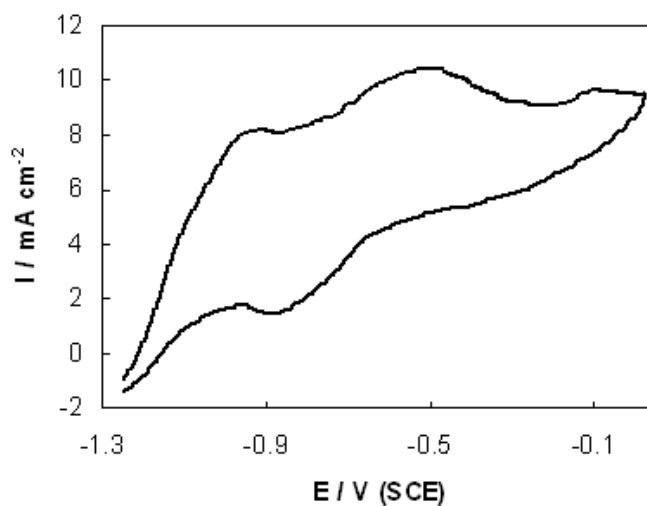


Figure 16. Cyclic voltammogram for NPG-coated Au wire array on a planar Au film in 1.0 mol dm⁻³ NaOH containing 0.02 mol dm⁻³ AB at 10 mV s⁻¹.

Conclusions

It has been shown that the characteristics of AB oxidation at Au electrodes are strongly influenced by electrode morphology. The data summarized in Table 1 indicates that the oxidation current for AB increases from 2.5 mA cm⁻² for a planar Au film to 13.1 mA cm⁻² for NPG wire array, while the onset of oxidation shifts from -1.02 V to -1.30 V vs SCE. Attempts were made to enhance the stability of NPG wires by either reinforcing the NPG wires with a Au wire core or by anchoring NPG wires onto Au wires. NPG wires supported on a Au wire array showed comparable electrocatalytic activity to a NPG-only wire array while reinforcing NPG with a Au core led to a slight decay in electrocatalytic activity.

Table 1 Variation of AB oxidation onset potential and maximum current density at a range of Au substrates

<u>Substrate</u>	<u>AB onset potential / V vs SCE</u>	<u>I max / mA cm⁻²</u>
Planar Au	-1.02	2.5
Au wire array	-1.13	5.2
NPG on planar Au	-1.20	3.1
NPG wire array	-1.30	13.1
NPG-coated Au wire array	-1.21	10.5
NPG wires supported on Au wire array	-1.28	12.7

Our findings will provide useful information in identifying a viable anode catalyst for the oxidation of an environmentally friendly, high energy density alternative fuel.

Acknowledgments

This work is supported by Irish government funding; it is part of an EPA STRIVE research fellowship entitled “Zero Carbon Emission Micro Fuel Cell Design”; Contract No. 2007-FS-ET-6-M5.

References

1. M. Chandra, Q. Xu, *J. Power Sources*, **168**, 135 (2007).
2. Q. Xu, M. Chandra, *J. Alloys and Compounds*, **446–447**, 729 (2007).
3. X. Zhang, S. Han, J. Yan, H. Shioyama, N. Kuriyama, T. Kobayashi and Q. Xu, *Int. J. Hydrogen Energy*, **34**, 174 (2009).
4. X. Yang, F. Cheng, J. Liang, Z. Tao and J. Chen, *Int. J. Hydrogen Energy*, **34**, 8785 (2009).
5. R. P. Shrestha, H. V. K. Diyabalange, T. A. Semelsberger, K. C. Ott and A. K. Burrell, *Int. J. Hydrogen Energy*, **34**, 2616 (2009).
6. B. Molina Concha and M. Chatenet, *Electrochimica Acta*, **54**, 6119 (2009).
7. G. Wolf, J. Baumann, F. Baitalow, F. P. Hoffmann, *Thermochim. Acta*, **343** 19 (2000).
8. J. Baumann, F. Baitalow, G. Wolf, *Thermochim. Acta*, **430**, 9 (2005).
9. A. Gutowska, L. Li, Y. Shin, C. M. Wang, R. S. Smith, B. D. Kay, B. Schmid, W. Shaw, M. Gutowski, T. Autrey, *Angew. Chem. Int. Ed.*, **44**, 3578 (2005).
10. S. D. Benedetto, M. Carewska, C. Cento, P. Gislou, M. Pasquali, S. Scaccia, P. P. Prosini, *Thermochim. Acta*, **441**, 184 (2006).
11. X. Zhang, J. Yan, S. Han, H. Shioyama and K. Yasuda, *J. Power Sources*, **182**, 515 (2008).

12. C. Yao, H. Yang, L. Zhang, X. Ai , Y. Cao and J. Lao, *J. Power Sources*, **165**, 125 (2007).
13. L. C. Nagle and J. F. Rohan, *J. Electrochem. Soc.*, **153**, C773 (2006).
14. A. J. Forty, *Nature* **282**, 597 (1979).
15. K. Sieradzki and A. Karma, *Nature* **410**, (2001).
16. F. Tian and C. Xu, *J. Am. Chem. Soc* **129**, 42 (2007).
17. L. Liu and R. Scholz, *Nanotechnology* **19**, 335604 (2008).
18. R. Zeis, *Journal of Catalysis* **253**, 132 (2008).